NUMERICAL AND EXPERIMENTAL INVESTIGATIONS OF TRANSIENT TEMPERATURE DISTRIBUTION IN FRICTION STIR SPOT WELDING OF ALUMINUM ALLOY AA6061

Asst. Prof. Dr. Mohsin N. Hamzah

Mechanical Eng. Dept. University of Technology 20066@uotechnoloy.edu.iq

Asst. Prof. Dr. Sadeq H. Bakhy

Mechanical Eng. Dept. University of Technology sadaqbakhy@yahoo.com

Mujtaba A. Fliayyh

Mechanical Eng. Dept. University of Technology mujtabaabdulkadhim@ gmail.com

Abstract

Friction stir spot welding (FSSW) is a powerful and superior alternative to resistance spot welding and riveting for fabrication of aluminum sheet metal structures. The objective is to study the variation of transient temperature in a friction stir spot welded plate of AA6061 Aluminum Alloy. Numerical and experimental investigations were performed to study the temperature distribution during this process. Two thermocouples (type K) were placed at two specified locations from the pin hole to measure the transient temperature during FSSW welding process. Numerically, 3D finite element model was built using ANSYS workbench Ver.15 to simulate the thermal model during welding. The torque and axial load were measured experimentally to determine the coefficient of friction, which used with the other parameters, to find the applied heat flux for the welding process. The temperature distributions of the specimens welded by three tools with different pins; i.e. cylindrical, tapered and triangular, at constant other FSSW parameters, were investigated and compared with the experiment temperature measured using the thermocouples to validate the results. The results show that the temperature produced from the welded specimen with cylindrical pin shape has the highest temperature distributions due to high axial load and torque as compared with other tool pin profiles. Also the results show good agreement between numerical and experimental with a percentage error (-3.09 – 7.83) %.

الدراسات العددية والعملية لتوزيع درجة الحرارة العابرة في اللحام الاحتكاكي النقطي لسبيكة الألومنيوم AA6061

الخلاصة:

طريقة اللحام الاحتكاكي النقطي هي طريقة لحام متطورة نسبيا وتستخدم كطريقة بديلة وفعالة للحام الكهربائي وطريقة الوصلات اللتان يستخدمان للحام الالمنيوم. ان الهدف الرئيسي من هذا البحث هو اجراء دراسة عملية ونظرية لتوزيع الحرارة المتولدة خلال اللحام الاحتكاكي النقطي لسبيكة الألومنيوم AA6061-T6 وذلك لفهم الظاهرة الفيزيائية الناتجة من خلال اختراق اداة اللحام للعينات المراد لحمها. تم استخدام ثرموكبلين نوع K ثبتت على مسافة 4 mm و 7 mm من مركز ادارة اللحام لقياس الحرارة المتولدة اثناء اللحام. نظريا تم انشاء موديل باستخدام (ANSYS workbench Ver.15) لمحاكاة توليد الحرارة. في هذا الموديل تم قياس الحمل المحوري والعزم المتولدة اثناء عملية اللحام تجريبيا لانهما يستخدمان في حساب معامل الاحتكاك الذي يستخدم مع متغيرات اخرى لايجاد تدفق الحرارة في عملية اللحام.في هذه الدراسة تم تغيير شكل اداة اللحام اسطواني ومخروطي ومثلثي وثبتوت عوامل اللحام الاحتكاكي النقطي الاخرى.اظهرت النتائج ان توزيع درجة الحرارة المتولدة باستخدام اداة لحام ذات شكل اسطواني هي الاعلى في توزيع درجة الحرارة و ذلك بسبب ارتفاع الحمل المحوري والعزم المسلط عند مقارنتها بادوات اللحام الاخرى. وكذلك هناك تقارب جيد بين انتائج النظرية العملية و بنسبة خطا بين (%)(7.83-3.09-

الكلمات المفتاحية: اللحام الاحتكاكي النقطي، سبيكة الألومنيوم AA6061-T6 ، توزيع درجة الحرارة

1. Introduction

Recently, a variant of the "linear" friction stir welding, called Friction Stir Spot Welding (FSSW), has been developed and implemented in automotive industry as a replacement of resistance spot welding for aluminum. FSSW is a new solid-state joining process able to weld similar and dissimilar overlap joints in different classes of materials with a reduction of energy consumption and capital costs of, approximately, 85% and 50% as compared resistance spot welding [1]. The FSSW process consists of three phases; plunging, stirring, and retraction, as depicted in Figure (1). The tool geometries, i.e. shape and diameter of both tool pin and shoulder and welding parameters such as spindle rotational speed, axial feed rate, dwell time, and plunge depth exert significant effect on the microstructures and mechanical properties of the friction stir spot welded joints.

The increasing application of this welding technology has urged many researchers to study several aspects, such as the determination of optimal sets of process parameters, the mechanical strength and the microstructural properties of the joints, e.g. Sun et al. Babu et al. [2], Ikuta et al. [3], Mahmoud et al. [4], Paider et al. [5] and Sun et al. [6]. Babu et al. [6] conducted FSSW experiments on 3mm thick sheets of aluminum alloy 2014 in T4 and T6 conditions, with and without Alclad layers. They produced welds using several different tools over a broad range of process parameters to evaluate their influence on bond width and hook formation. The effects of Alclad layers and base material temper condition were investigated. Lap-shear and cross-tension tests were conducted on joints produced by FSSW and riveting. Failure modes in friction stir spot welds were analyzed

. Ikuta et al. [3] investigated the influence of the tool shape, i.e. threaded, half threaded and no threaded on the mechanical properties and microstructural feature on the dissimilar aluminum alloy (Al 5754/Al 6111) lap joint friction stir spot welding. Mahmoud et al. [4] performed FSSW on annealed aluminum alloy AA5754 sheets. They presented the influence of these parameters on the weld structure included width of the bond region and microstructure of the weld region. Paider et al. [5] who investigated the effect of the shoulder penetration depth and the rotational speed on the friction stir spot welding of 2024-T3 aluminum alloy on the surface appearance, macrostructure, temperature profile, maximum failure load, and failure fracture modes. Sun et al. [2] investigated the influence of tool design and tool rotational speed variations on the torque, energy output, stir zone temperature and average grain size in the stir zones of magnesium alloy (AZ31) friction stir spot welds

Other researchers used the finite element methods to simulate the welding process, especially the works by Urso et al. [7], Gao et al. [8], and Awang et al. [9]. Urso et al. [9] carried out simulation study of FSSW process for the lap-joining of thin aluminum sheets using the FEM code, DEFORM 2D. They performed a set of experiments by on AA6060-T6 aluminum alloy plates using rotational speed, axial feed rate and plunging depth. Gao et al. [8] presented the results of a FE analysis of the FSSW process of AA6082-T6 considering geometric dynamic recrystallization. They used commercial FE package, DEFORM-3D, to predict the dislocation density, Grain size, temperature, effective strain, and strain rate during FSSW. They also achieved an experimental work and compared it with the numerical one to validate the result. Awang et al. [7] developed a finite element model of friction stir spot welding of 6061-T6 aluminum alloy and analyzed the energy generation during modeling process. They developed a three dimensional finite element coupled thermal-stress model of FSSW in Abaqus/Explicit code. Moreover, they analyzed the temperature profile and energy dissipation history of FEM.

The main objective of this paper is to study the distribution of transient temperature during FSSW process used for welding AA6061 aluminum alloy plate. To achieve this objective numerical and experimental investigations were performed to validate the result.

2. Experimental Work
2.1 Welding equipment and conditions
AA 6061-T6 aluminum alloy sheets with thickness of 1.6 mm were used to produce FSSW lap joints. The chemical compositions and mechanical properties of these Al alloys sheets are given in Tables 1 & 2. Vertical CNC milling machine type "C-tek" equipped with special fixture for FSSW was used. In this work, FSSW was conducted with three different tool pin shapes, the other welding parameters were kept constant, i.e. rotational speed of 1200 rpm, plunging depth of 2.8 mm, plunging rate of 15 mm/min, and dwell time of 11.2 sec. The pin tool shapes are; cylindrical, tapered, and triangular, Figure (2).

2.2 Measuring the Transient Temperature Distribution
During FSSW process, the plate prepared to measure transient temperature by using thermocouples at two locations. The two plates and thermocouples assembled with the backing plate prepared for this purpose. on the bottom welded plate, 1.5 mm diameter holes drilled to place thermocouples which have diameter 1mm. Type K thermocouples, with temperature range of -100 ℃ to 1100 ℃, were inserted in the holes and glued with an isolator to ensure intimate contact with the bottom welded plate and to prevent the contact with the backing plate. The temperature was measured in two locations, heat affected zone and thermo-mechanical heat affected zone, Figure (3). The thermocouples are connected to the reader which attached to the SD card data logger temperature recorder (BTM-4208SD) to measure the transient temperature, Figure (4).the speciman of the FSSW process shown in the figure (6).

2.3 Normal Load and Tool Torque Measurement
For measuring normal load and torque during the welding process, a special rig prepared by Mahmood H. M. et al. [11] for measuring the load and torque. The rig consists of two steel plates of dimensions 320×180 mm and thickness 25 mm, two guide columns and bushes at the center of upper plate, Figure (5). The upper plate sliding on the columns while the lower plate is fixed. The plates to be welded was fixed to the fixture and the last assembled with the

rotating disc constructed with the thrust bearing to withstand the axial load applied by the welding tool. Also, rotate freely to measure the torque of the tool. This assembly fixed to the sliding plate at its center. Load cell, SEWHA, R.O:2.000 mV/V, 1000 kg capacity, was fixed to the center of the lower clamping plate to support the upper moving plate and the welding fixture assembly. Another load cell, SEWHA, R.O:2.003 mV/V, 100 kg capacity, was fixed horizontally at the upper plate at a distance 45 mm from the fixture center and normal to it, to measure the applied torque.

3. Thermal Model

In the present study a commercial general purpose finite element software ANSYS 15.0 workbench was used for numerical simulation of friction stir spot welding process. In the thermal analysis, the transient temperature, which is a function of spatial coordinates (x, y, z) and time t, are estimated by the three dimensional nonlinear heat transfer equation [1],

$$k(T)\left(\frac{\partial^2 T}{\partial x^2} + \frac{\partial^2 T}{\partial y^2} + \frac{\partial^2 T}{\partial z^2}\right) + Q_{int} = c(T)\,\rho(T)\,\frac{\partial T}{\partial t} \tag{1}$$

Where t is the time, T is the absolute temperature, Q_{int} is the internal heat source rate (rate of heat generation) k temperature dependent thermal conductivity coefficient of the workpiece, c is temperature dependent specific heat of workpiece, and ρ is temperature dependent density of the workpiece

3.1 Assumptions

Modeling of the actual physical phenomena of the FSSW process is rather complicated. Therefore, the following assumptions have been made.

1. Material is isotropic and homogeneous.
2. No melting occurs during the FSSW process.
3. Initial temperature is assumed to be T_o =25 $^{\circ}$C.
4. 100% of the dissipated energy due to friction is assumed to be transformed into heat.

3.2 Geometry

In the 3D numerical model, SOLIDWORKS 2015 was used to draw the model which consists of two welded plates. Each welded sheet has dimensions of 100×25 mm and thickness 1.6 mm, the overlap area was 25×25mm, as shown in Figure (6 A).

3.3 Mesh Generation

One of the most relevant steps in the Finite Element Analysis is meshing. The accuracy and speed of the results have a direct contact on how this part is done. The higher the numbers of nodes are the higher the accuracy of the results, however the speed of the simulation decreases. The workpiece was divided into 70260 elements and 118815 nodes and the element size is 1.e-003 m, Figure (6 B)

3.4 Material Properties

Thermal properties of the material, such as density, thermal conductivity, and specific heat are temperature dependent. An accurate determination of welding temperatures is critical due to

the stresses and strains developed in the welding process, which are temperature dependent. Therefore, temperature dependent thermal properties of AA6061-T6 Aluminum alloy were used in FE model. The material properties of this alloy are shown in Table 3. These thermal properties values are obtained from reference [13], and for higher temperatures, their values are linearly extrapolated.

3.5 Boundary Conditions

Boundary conditions for FSSW model were specified as surface loads through ANSYS workbench Ver. 15. Assumptions were made for various boundary conditions based on data collected from references [14, 15 and 16].

Convective and radiative heat losses to the ambient occur across all free surfaces of the workpiece, and conduction losses occur from the workpiece surfaces to the backing plate and upper clamping disc.

To consider convection and radiation on all workpiece surfaces, the heat loss q_s was calculated by equation:

$$q_s = \beta\,(T - T_o) + \eta\,\xi\,\varepsilon\,(T^4 - T_o^4) \qquad (2)$$

where T is the absolute temperature of the workpiece, T_0 is the ambient temperature, β is the convection heat transfer coefficient, ε is the emissivity of the plate surfaces, η is radiation view factors, and $\xi = 5.67 \times 10^{-12}\ W cm^2\ °C$ is the Stefan-Boltzmann constant. In the current model, a typical value of β was taken to be equal to 30 w/m^2 °C using an ambient temperature of 300° K, ε was taken to be 0.5, and $\eta = 1$ for aluminum [17].

In order to account for the conductive heat loss through the bottom and upper surfaces of weld sheets, a high overall heat transfer coefficient was assumed. The heat loss was modeled approximately by using the heat flux loss by convection q_b given by equation (3).

$$q_b = \beta_b\,(T - T_o) \qquad (3)$$

where β_b is a fictitious convection coefficient. Due to the complexity involved in estimating the contact condition between the sheet and the plates, in this study, the optimized value of β_b was assumed to be 418 w/m^2 k [13]

3.6 Friction Stir Welding Tool

The friction stir welding tool was fabricated from X12M tool steel, density ρ=7800kg/m3, specific heat Cp=500J/kg.°C and thermal conductivity k=40w/m.°C. The tool has a flat shoulder; while the tool pin has three profiles, i.e. cylindrical, tapered and triangular. The overall height of the pin is 2.5 mm, making it slightly shorter than the sheets thickness and the shoulder plunges 0.3 mm on in the welded plate. Figure (7), is illustrating the configuration of the tool used in the welding process.

3.7 Heat Generation in Friction Stir Spot Welding

Heat generation and the elevation of the surface temperatures are generally related with friction that transforms kinetic energy into thermal energy. The energy generated resulted from the tangential reaction force acting over a distance. In general, the energy from friction work is expressed as,

$$E = \mu_K \int_0^L F_n\,(x)\,dx \qquad\qquad (4)$$

where, E is the energy generated, μ_k is the kinetic friction coefficient, F_n is the friction force, and x is the distance of an object moved. According to reference [13], about 90-95% of the energy due to friction is converted into heat and about 5-10 % of the remaining energy causes deformation of the material and some stores as defects in the touching material.

In FSSW process, friction work, which is generated due to the difference between the velocity of the rotating tool and the stationary workpiece, produces heat energy. Friction work at the tool and the workpiece interface can be classified into three groups based on tool geometry, heat generated from the pin tip, heat generated from the vertical side of the pin and heat generated from the shoulder surface as shown in Figure (8).

Each contact surface experiences sliding friction during friction stir spot welding process. The total heat generated by friction work, at the tool and the workpiece interface is the summation of the heat generated at the contact surface of the shoulder, the tip of the pin, as well as the side of the pin. For this case, the shoulder and the tip of the pin are flat.

The energy generation during friction stir spot welding represents heat generation due to plastic deformation and heat due to friction between the tool and workpiece. Nandan et al. [16] utilized the slip factor (δ) to represent the partition of the heat from plastic deformation, i.e. this factor ranged from 0.6 to 0.85. On the other hand, the heat generated from friction was calculated from the torque produced.

First, the heat generated from the shoulder can be computed from torque formula. The total torque at the interface of the shoulder can be expressed as

$$T_{Shoulder} = \int_{R_i}^{R_o} dM = \int_{R_i}^{R_o} \sigma_{contact}.r.(2\pi.r)dr \qquad\qquad (5)$$

where, $T_{Shoulder}$ is the torque at the shoulder interface, $\sigma_{contact}$ is the contact shear stress, r is the distance from the tool axis, and R_o and R_i is the radii of the shoulder and the pin, respectively. Solving equation 5, yields,

$$T_{Shoulder} = \frac{2}{3}\pi\sigma_{contact}(R_O^3 - R_i^3) \qquad\qquad (6)$$

The power produced to the workpiece is,
$$P = T.\omega \qquad\qquad (7)$$

where, $\omega = 2\pi n$, n is the angular velocity of the tool (rev. per second).

$$T_{Shoulder} = \frac{4}{3}\pi^2\sigma_{contact}.n(R_O^3 - R_i^3) \qquad\qquad (8)$$

Since $\sigma_{contact} = \mu\sigma$, where σ is the contact pressure and μ is coefficient of friction. Equation (8) becomes:

$$T_{Shoulder} = \frac{4}{3}(1-\delta)\,\pi^2\mu\sigma.n(R_O^3 - R_i^3) \qquad\qquad (9)$$

The heat generated by the friction work at the tip of the pin and the workpiece interface, P_P can be obtained by similar approach.

$$P_P = \frac{4}{3}\pi^2(1-\delta)\,\mu\sigma.nR_i^3 \qquad\qquad (10)$$

The total torque at the vertical pin surface, $T_{pin(v)}$ can be expressed as

$$T_{pin(v)} = \int_0^l \sigma_{\text{contact}} . R_i . (2\pi . R_i) dy \qquad (11)$$

Where *L* is the height of the pin. Solving equation 11, yields

$$\text{T}_{\text{pin(v)}} = 2\, \sigma_{\text{contact}}\, \pi.\, \text{L}.\, \text{R}_\text{i}{}^2 \qquad (12)$$

Substituting equation (12) in equation (7), also substitute ω = 2πn and $\sigma_{\text{contact}} = \mu\sigma$ the heat produced at the vertical pin surface, P $_{\text{pin (v)}}$ becomes:

$$P_{pin(v)} = 4\, \pi^2\, \mu\, \sigma\, n.\, L.\, R_i{}^2 \qquad (13)$$

During FSSW process, the tool travels at constant plunge speed across the welded plate. The motion of the tool is simulated by changing the heat source location. The dwell time in FSSW process is 11 sec, while the tool of shoulder plunge a distance equal to 2.8 mm. The dwell time, obtained from the plunging depth and plunging speed, divided into four steps, i.e. 2.8 sec, 5.6 sec, 8.4 sec and 11.2 sec. For any time step, the heat flux is applied at the tip surface of the pin and vertical side surface of the pin, i.e. for dwell time 2.8 sec the pin plunge a distance of 0.7 mm and the heat flux is applied for the tip surface and vertical surface with length 0.7mm

In the same context for the dwell time 5.5 sec and 8.25 sec, the pin plunged a 1.4 mm and 2.1 mm, respectively.   Also the heat flux at the pin tip and vertical surface was varied according to the length of pin, the vertical surface becomes 1.4 mm and 2.1 mm. For dwell time 11.2 sec, the pin plunges a 2.5 mm and the shoulder plunges 0.3 mm across the welded plate. In this stage, the heat flux applied at the pin and vertical surface of the pin with surface length 2.5 mm and also at the tip surface of the shoulder, Figure (9).

4. Results and Discussion
4.1 Axial Load and Torque Results in FSSW

During the FSSW process, the torque and load were measured by using special rig with load cells prepared for this purpose [11]. The load and torque were measured for three pin profiles; triangular, tapered and cylindrical with tool rotational speed 1200 rpm.

4.1.1 Axial Load Results in FSSW

Figure (10-A) shows the load applied for FSSW with cylindrical pin. The axial load increased at constant rate until a certain point, then the axial load decreased dawn and finally the load began to increase again. The breaking point in which the load decreased represent the state when the pin generated enough heat in the upper plate. The material flow stresses reduced which eases the flow of material; therefore, the load decreases. The decrease in axial load was held for short time and then the axial load began to increase once again, due to the tool reaches to the lower plate, i.e. plunge depth 1.6mm. Also, further increase in axial load occurs at plunging depth 2.2 mm (when the shoulder starts to plunge across the upper plate).

For the tapered and triangular pin, the axial load behavior results from FSSW process similar to the behavior for the cylindrical pin due to the same of the plunging depth for the pin and shoulder. Figure (10-B) and Figure (10-C) show the axial load curve for these pins profile.

Among the three behavior of the axial load, as shown in Figure (10-D), the tool with cylindrical pin has the maximum load curve due to the surface projected area of the pin tip

being larger than tip surface of the other tools. Also, the axial load curve of the tapered pin tool has values less than cylindrical pin shape. The tool with triangular pin has the lowest values as compared with other pin profiles.

4.1.2 Toque Results in FSSW Process

The variation of the torque of the FSSW tool represents the shear stresses acting on it. For the cylindrical pin profile, as shown in Figure (11-A), the torque initially increased as the tool plunging depth increased until the plunging depth becomes 0.5 mm. After plunging depth of 0.5 mm the torque increases in slow rate, then the initial increasing because of the reduction of the flow stresses, in this stage, the heat generated enough heat that eases material flow. The torque increased with additional increase in tool plunging depth until plunging depth becomes 1.6 mm. In this plunging depth the tool pin becomes in contact with the lower plate which causes further increase in torque. The maximum value of the torque occurs when the shoulder becomes in contact with the upper plate, i.e. plunging depth 2.5 mm.

For the triangular pin profile, as shown in Figure (11-B), the same torque behavior for the cylindrical pin was gotten, except for plunging depth between 0.5mm and 1.6 mm, the torque increases at slower rate than that for the cylindrical pin. On the other hand, for tapered pin the increase in torque results from two reasons, i.e. increasing the plunging depth and increasing the area plunges the welded specimen, Figure (11-C) shows the curve of the torque for tapered pin.

More importantly, the torque of the tool with cylindrical pin was significantly higher throughout the plunging stage as compared with that on the tool with tapered and triangular pins. The torque of the triangular pin has lower value than cylindrical and tapered pin. Lower torque in welding process is generally considered beneficial in friction stir welding due to reduced consumption of power and increasing the life of the tool during welding process [6].

4.2 Temperature Distributions

During the FSSW process, the tool plunged 2.8 mm through the welded plates, i.e. the pin and shoulder plunged a depth of 2.5mm and 0.3mm, respectively. ANSYS workbench software was used for the simulation of the thermal analysis during welding process. The temperature gradient in two probes, placed in the lower surface of the bottom plate, was determined in order to compare them with the temperature measured experimentally to validate the result.

The experiments were achieved by using three tools with different pin shapes, i.e. triangular, cylindrical and tapered profile. Heat transfer coefficients between the surface of the lower plate and vertical side surfaces of the two plate with the fixture is 300w/m² °C, conversion heat transfer coefficient with air is 30w/m² °C, ambient temperature $T_0 = 25$ °C, and slip factor δ=0.8. The coefficient of friction varied instantaneously and determined from the above equations, in which the value of the torque and axial load was measured experimentally by a load cells fixed in special rig designed for this purpose. The value of μ was varied as the pin depth changes because of the variation of the axial load and tool torque with plunging depth. Depending on the torque and axial load, which measured experimentally, the coefficient of friction was determined from the above variables. For all pin profile, i.e. triangular, cylinder and taper, the μ was determined for four plunging depth; 0.7 mm, 1.4 mm, 2.1 mm and 2.8 mm. Based upon the determined coefficient of friction (μ) and pressure (*P*) as well as other welding parameters such as tool rotational speed and shape of the pin, the heat generation (Q) was determined and used as input load to model in ANSYS

workbench to estimate the distribution of the temperature in the welded plates, Table 4 through 6.

Figures (12 through 14) present the isometric view of the welded plate with different plunging depths for three pin profiles, i.e. cylindrical, triangular, and tapered pin, respectively. The maximum temperature was placed in the region of pin and shoulder when plunged due to the fact which the maximum heat generated at this region. Figures (15) shows the measured temperature distribution of the welded plates for the three pins profiles. Two thermocouples were used to measure the gradient of temperature, which   placed at distance 4 mm and 7 mm, respectively, from the center of the spot. For all pin profiles, the temperature increase as the time increased, plunging depth increase, until the maximum temperature where the shoulder plunges the upper plate, and then the tool retracts the welded plate, and the temperature decrease to the steady state temperature.

The temperature profile of the cylindrical pin has maximum temperature because of the relatively higher torque and load resulted from higher contact area than the other pin profiles. High axial load torque causes more plasticity of the welded plate which increases metal flow and the global temperature of welded plate increases. On the other hand, the global temperature distribution of the tapered pin profile came after the temperature curve distribution of the cylindrical pin profile. Also, the torque and axial load as in tapered pin instantaneous increased in area of the pin, as it plunged the welded plate, influence increasing the temperature gradient. Triangular pin profile has the lowest temperature values than the temperature results from other pins. Figure (16) shows the comparison of the temperature profile of the three pin shapes.

Figures (17) through (19) show a comparison of the experimental results with the ANSYS model in order to validate the results. It is noticed from these figures that there are reasonable differences between temperature curves due to several assumptions which affects the result of ANSYS model such as slip factor which represent the amount of deformation of material occurs during welding process and other assumptions explained above.

5. Conclusions

To study the variations of transient temperature in friction stir spot welding of aluminum alloy AA6061 plates, detailed three-dimensional nonlinear thermal and thermo-mechanical simulations are performed for the FSSW process using the finite element analysis. The investigations were consisted of numerical simulation and experimental work to study the temperature distribution during this process. From the analyses, we can summarize the results as follows:

1. In the current study, experimental work showed that AA6061-T6 aluminum alloy is weldable by FSSW using different tool pins shapes (i.e. cylindrical, tapered and triangular), the other welding parameters are kept constants.

2. For estimating the temperature distributions of the FSSW welded plates, the torque and axial load are used with the other parameters to calculate the heat flux which applies as a load in the ANSYS workbench model. Among the axial load and torque of three pin profiles tools, cylindrical pin has significantly higher load and torque throughout the FSSW process as compared to that on the tool with tapered and triangular pin profiles. Lower torque is beneficial because of consequence reduction in power consumption.

This, also, increased the tool life; therefore, the most efficient tool in the current work is found to be the tool with the triangular pin profile.

3. The type of pin profile has a direct effect on the temperature distribution during FSSW process, and is directly proportional to the areas of pins.

4. Among the three pin shapes, the temperature distributions of the specimen welded by cylindrical pin has the maximum values, followed by specimen welded by tapered pin. The plates welded by triangular pin have the lowest temperature distributions.

5. In ANSYS workbench, with nonlinear thermal model, the heat flux was used as input load. The results showed that the current numerical simulation is powerful and gave good agreement with experimental work, i.e. the percentage error ranged between (-3.37-10.41)%, and we suggest and recommend using this analysis for simulating the temperature distributions in friction stir spot welding process.

References

[1]   Hancock, R., "Friction welding of Aluminum Cuts Energy Cost by 99%", *Welding Journal*, vol. 83, 2004.

[2]   Babu S., Sankar V.S., Janaki G.D., Venkitakrishnan P.V., Reddy G. M., Rao K.P., "Microstructures and Mechanical Properties of Friction Stir Spot Welded Aluminum Alloy AA2014", *Journal of Materials Engineering and Performance Vol. 22, No. 1, 2013*.

[3]   Ikuta A., Yin Y.H., North T.H., "Influence of Tool Thread on Mechanical Properties of Dissimilar Al Alloy Friction Stir Spot Welds", *Science and Technology of Welding and Joining*, Vol.17, No.8, 2012.

[4]   Mahmoud T.S., Khalifa, T.A., "Microstructural and Mechanical Characteristics of Aluminum Alloy AA5754 Friction Stir Spot Welds", *Journal of Materials Engineering and Performance*, Vol. 23, No.9, 2014.

[5]   Paidar M., Khodabandeh A., Najafi H., Sabour A., "Effects of the Tool Rotational Speed and Shoulder Penetration Depth on Mechanical Properties and Failure Modes of Friction Stir Spot Welds of Aluminum 2024-T3 Sheets", *Journal of Mechanical Science and Technology*,Vol.28, No. 12, 2014.

[6]   Sun N., Yin Y.H., Gerlich A.P., North T.H., "Tool Design and Stir Zone Grain Size in AZ31 Friction Stir Spot Welds", *Science and Technology of Welding and Joining*, Vol. 14, No. 8, 2009.

[7]   D'Urso G., Giardini C., "FEM Model for the Thermo-Mechanical Characterization of Friction Stir Spot Welded Joints", *International Journal of Material Forming*, Aluminum Association, MATTER. Project, 2001.

[8]   Z. Gao, Niu J., Krumplials F., Enziner N., Mitsche S., Soniinitsch C., "FE Modelling of Microstructure Evolution During Friction Stir Spot Welding In AA6082-T6", *Weld World*, Vol. 57, 2013.

[9]   Awang M., Mucino V.H., "Energy Generation during Friction Stir Spot Welding (FSSW) of Al 6061-T6 Plates," *Materials and Manufacturing Processes*, Vol.25, 2010.

[10]   http://aluminium.matter.org.uk/aluselect/09_mech_browse.asp.

[11]   Mahmood H.M., Hassan S. S., Tolephih M. H., "Experimental and Numerical Study of a New Improved Friction Stir Spot Welding for Aluminum Alloy Sheets", *Ph.D. Thesis*, University of Technology. Mechanical Engineering Department, 2015.

[12]   Salloomi K.N., Sabri L. A., Hamad Y.M., Mohammed S.N.," 3-Dimensional Nonlinear Finite Element Analysis of both Thermaland Mechanical Response of Friction Stir Welded 2024-T3 Aluminum Plates" *Journal of Information Engineering and Applications*, Vol.3, No.9, 2013.

[13]   Awang M., "Simulation of Friction Stir Spot Welding (FSSW) Process: Study of Friction Phenomena" *Ph.D. thesis, Department of Mechanical and Aerospace Engineering, Morgantown, West Virginia,* 2007.

[14]   Zhu X.K., Chao Y. J., "Numerical Simulation of Transient Temperature and Residual Stresses in Friction Stir Welding of 304L Stainless Steel*", Journal of Materials Processing Technology*, Vol. 146, No. 2, Pages 263-272 ,2004.

[15]   Khandkar Z.H., Khan J.A., Reynolds, A.P., Sutton, M.A., "Predicting Residual Thermal Stresses in Friction Stir Welded Metals", *Journal of Materials Processing Technology*, Vol. 174, Pages 195-203, 2006.

[16]   Nandan R., Roy G. G., Lienert T.J., Deb Roy T., "Numerical Modelling of 3D Plastic Flow and Heat Transfer During Friction Stir Welding of Stainless Steel*," Science and Technology of Welding and Joining*. 11(5), pp., 526-537, 2006.

[17]   Longhurst W.R., "Force Control of Friction Stir Welding," Ph.D. *Thesis*, Nashville, Tennessee, 2009.

Table (1) Standard and actual chemical composition of aluminum alloy AA6061.

Percentage Composition	Si	Fe	Cu	Mn	Mg	Cr	Zn	Ti	Al
Nominal [9]	0.4-0.6	0.70 Max	0.15-0.4	0.15 Max	0.8-1.2	0.04-0.35	0.25 Max	0.15 Max	Balance
Actual	0.435	0.370	0.224	0.100	0.810	0.185	0.026	0.055	Balance

Table (2) Standard and actual mechanical properties of aluminum alloy AA6061

	σ_y	σ_u	EI %
Standard Value [9]	345	393	15%
Actual Value	356	405	16%

Table (3) Temperature dependent material properties for AA 6061-T6.

Temperature ^{o}C	Thermal Conductivity W/m^{0}C	Heat Cap. J/Kg ^{o}C	Density Kg/m^3	E (GPa)	Yield Strength. MPa	Thermal Expansion $10^{-6}/^0$C
37.80	162	945	2685	68.54	274.4	23.45
93.30	177	978	2685	66.19	264.6	24.61
148.9	184	1004	2667	63.09	248.2	25.67
204.4	192	1028	2657	59.16	218.6	26.60
260.0	201	1052	2657	53.99	159.7	27.56
315.6	207	1078	2630	47.48	66.2	28.53
371.1	217	1104	2630	40.34	34.5	29.57
426.7	223	1133	2602	31.72	17.9	30.71

Table 4 values of friction heating applied by tool with cylindrical pin[13].

Plunging Depth		T (N m)	P (MPa)	μ	Heat Generation (Watt/ m2)	
0.7 mm		2.8	222.4	0.42	Pin Tip	2.90e6
					Vertical side	5.25e6
1.4 mm		3.7	142.6	0.571	Pin Tip	4.60e6
					Vertical side	4.11e6
2.1 mm		4.5	147.6	0.793	Pin Tip	5.1608e6
					Vertical side	3.0719e6
2.8 mm	Pin	0.5	50.9	0.3	Pin Tip	1.53e6
					Vertical side	0.566e6
	Shoulder	12.3	33.74	0.42	1.8e6	

Table 5   values of friction heating applied by tool with tapered pin.

Plunging Depth	T (N m)	P (MPa)	μ	Heat Generation (Watt)	
0.7 mm	1	159.8	0.326	Pin Tip	1.86e6
				Vertical side	4.5e6

					Pin Tip	2.76e6
1.4 mm		1.8	116.3	0.623	Vertical side	4.8e6
2.1 mm		3	127.7	0.808	Pin Tip	4.09e6
					Vertical side	8.07e6
2.8 mm	Pin	0.5	76.39	0.25	Pin Tip	0.639e6
					Vertical side	1.26e6
	Shoulder	9.4	36.6	0.327	1.95e6	

Table 6   values of friction heating applied by tool with triangular   pin.

Plunging Depth		T (N m)	P (MPa)	μ	Heat Generation (Watt)	
0.7 mm		1.7	252.6	0.217	Pin Tip	5.69e6
					Vertical side	5.4e6
1.4 mm		1.8	233.7	0.235	Pin Tip	5.7e6
					Vertical side	2.829e6
2.1 mm		3	252.6	0.39	Pin Tip	9.49e6
					Vertical side	3.14e6
2.8 mm	Pin	0.5	126.6	0.2418	Pin Tip	3.17e6
					Vertical side	0.786e5
	Shoulder	11.3	35.6	0.416	2.01e6	

Table 7 results of both experimental and numerical of the maximum temperature with percentage error between them.

Pin Profile & Thermocouple Distance from the Spot Center		ANSYS Results	Experimental Results	Percentage error (%)
Cylindrical pin	4 mm	401.9	370.4	7.83
	7 mm	364.79	326.8	10.41
Tapered Pin	4 mm	329	340.1	-3.37
	7 mm	301.17	310.5	-3.097
Triangle Pin	4 mm	328.79	306.9	6.66
	7 mm	295.67	272.4	7.87
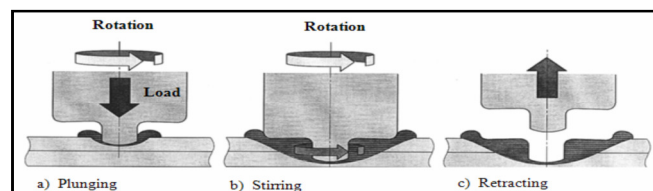
Figure (1) Friction stir spot welding (FSSW) process [1].

(A)

(B)

(C)
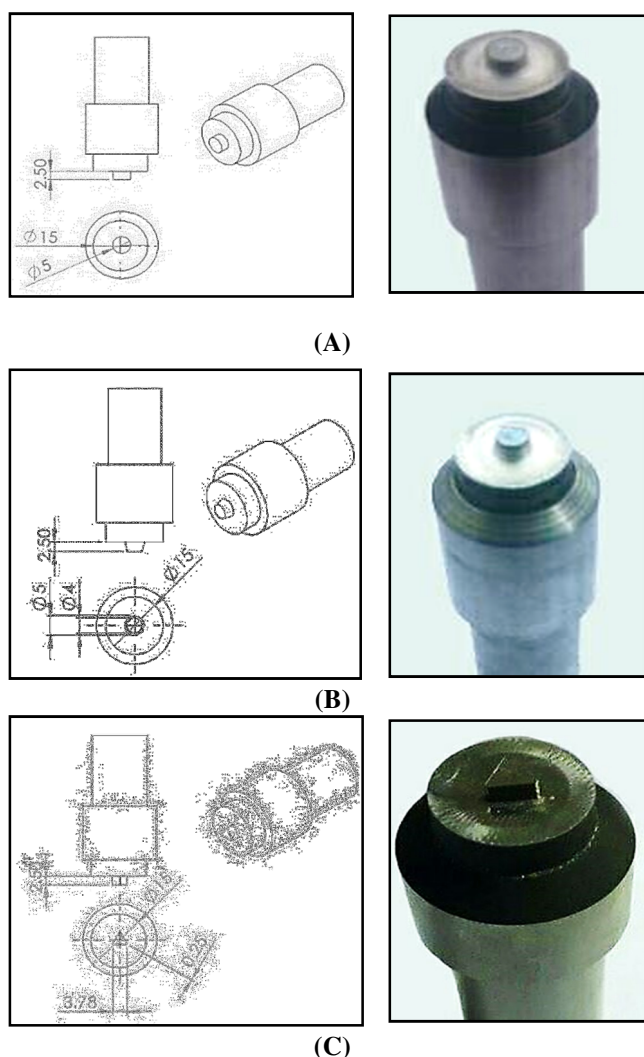
Figure (2) FSSW tool shapes: (A) cylindrical pin, (B) Tapered pin tool, and (C) Triangle pin tool (All dimension in mm).

(A)　　　　　　　　　**(B)**
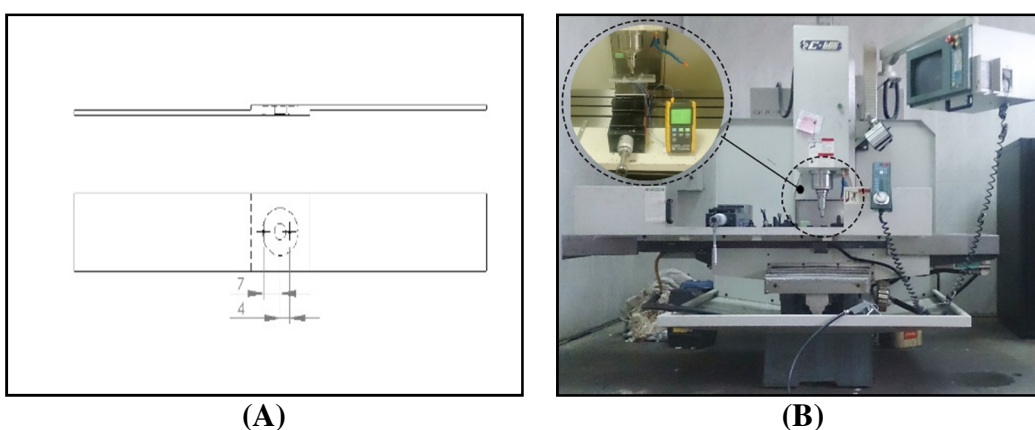
Figure (3) (A) Thermocouple position in the workpecie. (B)Temperature recorder and hole thermocouple position on workpiece.
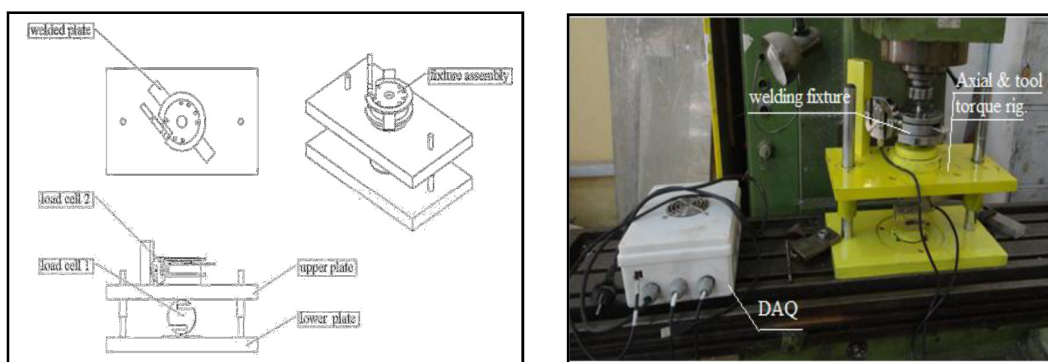
Figure (4) Assembly of the torque and load rig.

Figure (5) FSSW specimen.

| (A) | (B) |
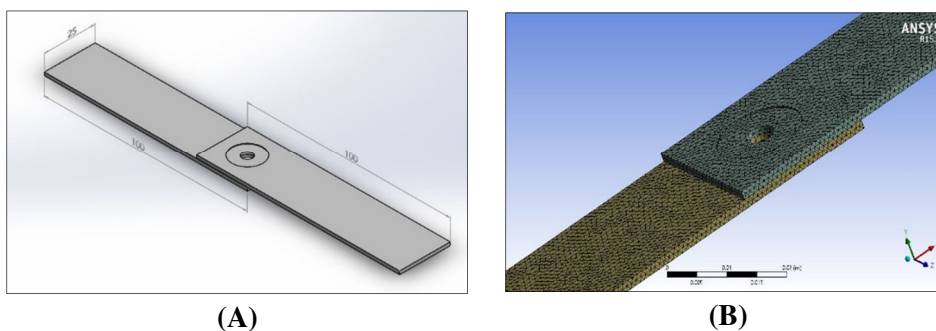
Figure (6) Finite element model and mesh of welded sheet.

| (A) | (B) | (C) |
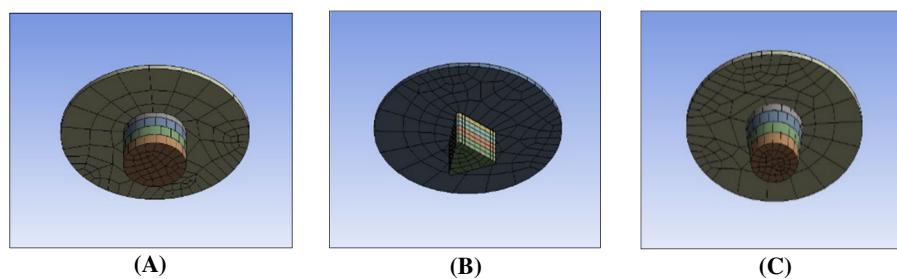
Figure (7) The tools used in FSSW process, (A) cylindrical pin, (B) triangular pin and (C) tapered pin.
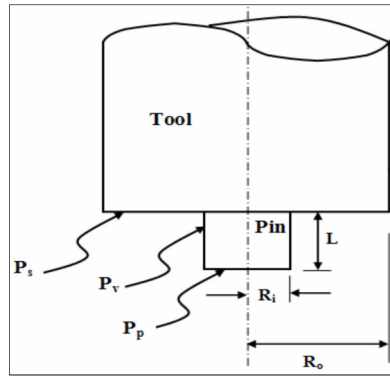
Figure (8) The heat distribution in the FSSW tool.

(A)

(B)

(C)

(D)
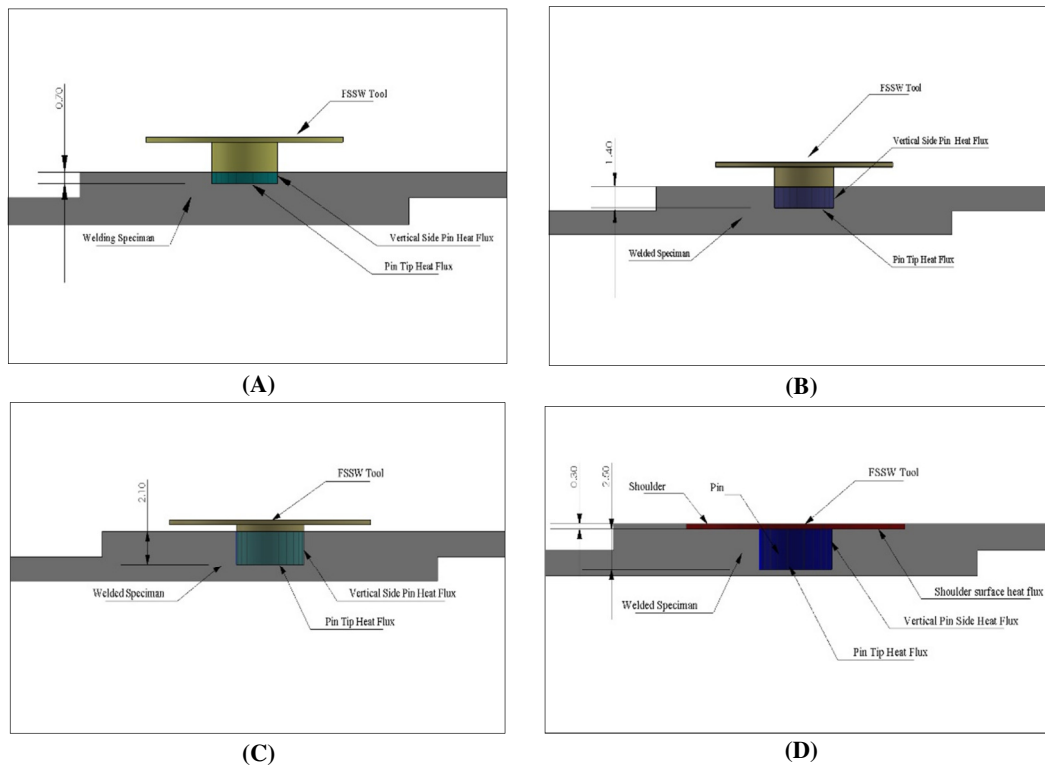
Figure (9) Applied heat flux for: (A) 0.7 mm, (B) 1.4 mm, (C) 2.1 and (D) 2.8 tool plunging depth.

(A)

(B)
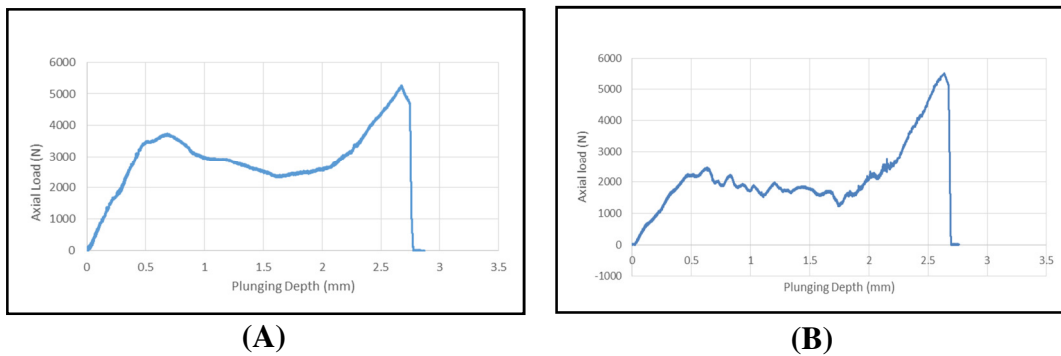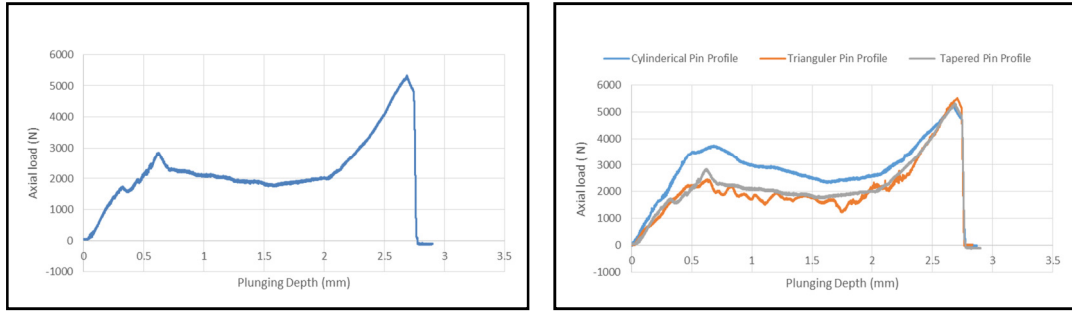
(C)   **(D)**

Figure (10) Axial load for the tool with: (A) cylindrical pin profile, (B) with triangular pin profile, (C) with tapered pin profile and (D) comparison of the axial load for the tool with above three pin profile.
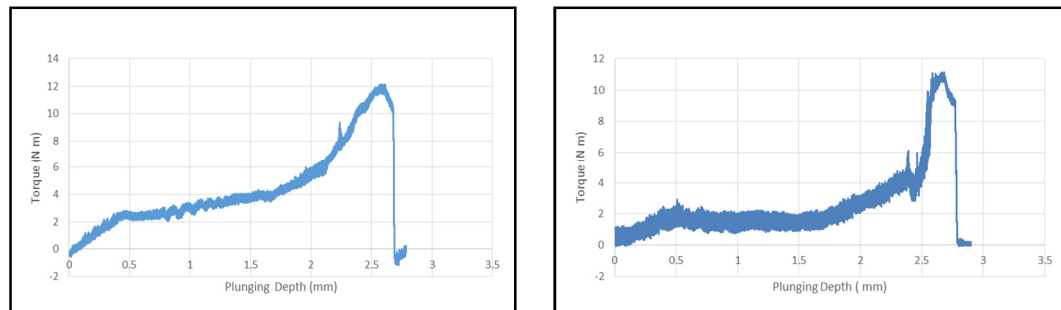
(A)   **(B)**
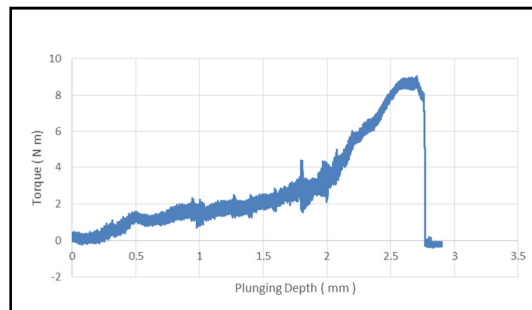
(C)

Figure (11) Torque applied for the tool with: (A) cylindrical pin profile, (B) with triangular pin profile, and (C) with tapered pin profile.

(A)   **(B)**

(C)

(D)
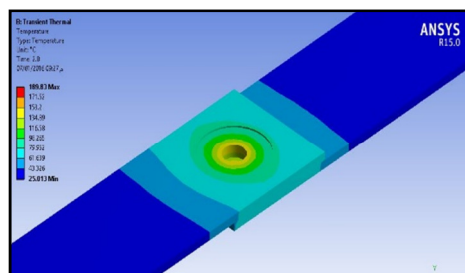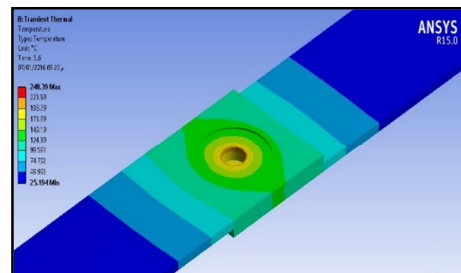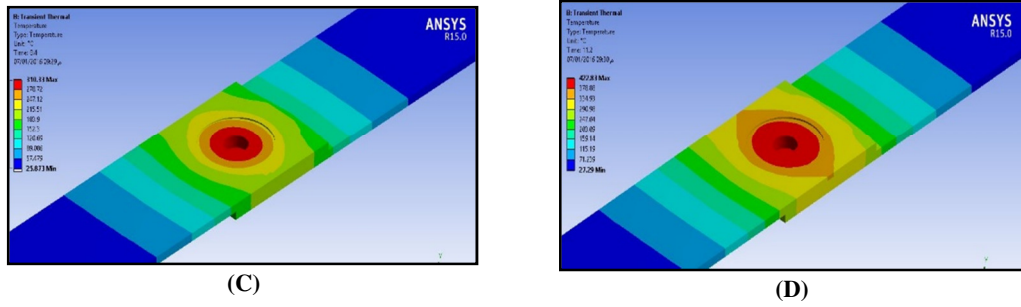
Figure (12) Isometric view for the welded plate and tool with tapered pin for different dwell time: (A) dwell time= 2.8 sec, (B) dwell time= 5.6 sec, (C) dwell time= 8.4 sec and (D) dwell time= 11.2 sec.


(A)

(B)

(C)

(D)
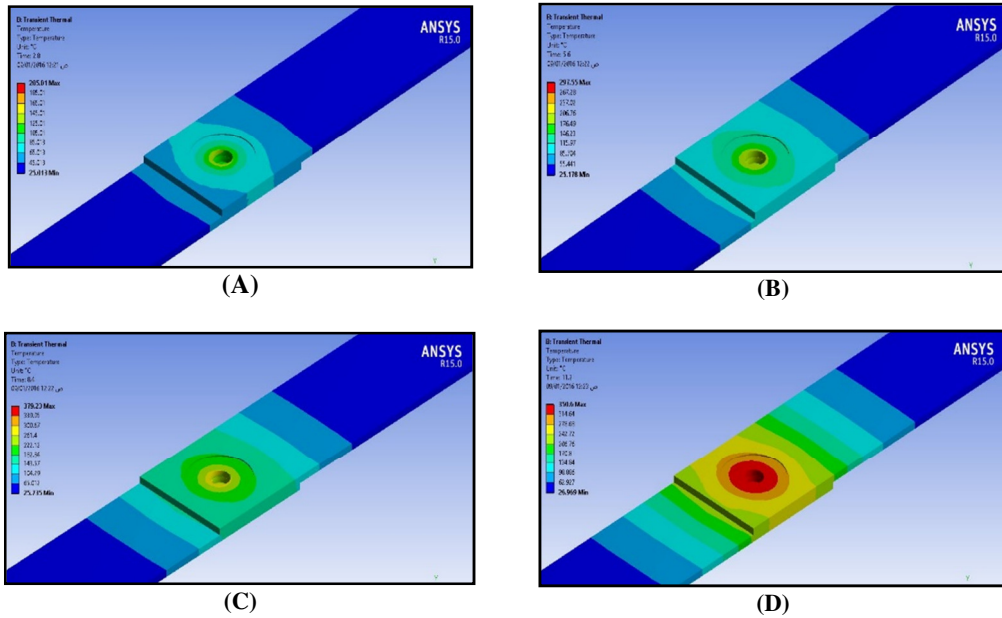
Figure (13) Isometric view for the welded plate and tool with tapered pin for different dwell time: (A) dwell time= 2.8 sec, (B) dwell time= 5.6 sec, (C) dwell time= 8.4 sec and (D) dwell time= 11.2 sec.

(A)

(B)

(C)   (D)
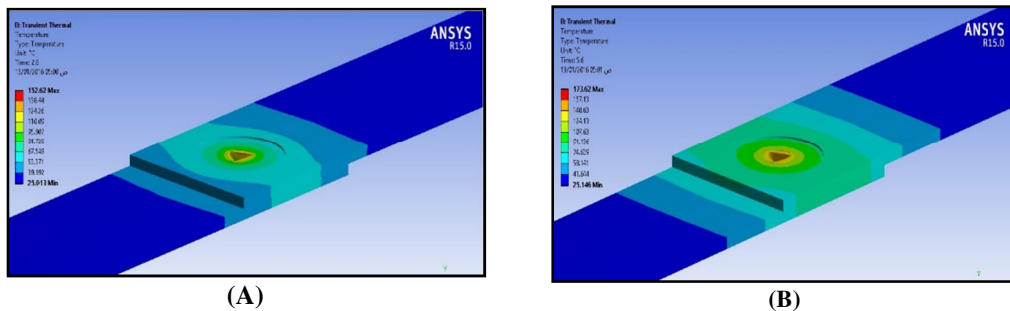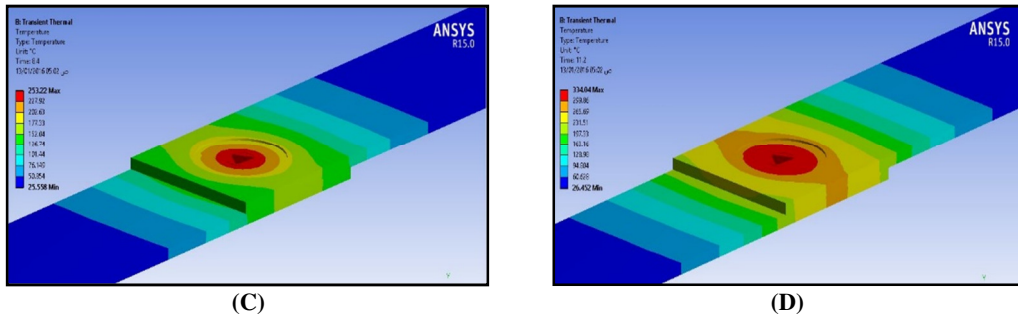
Figure (14) Isometric view for the welded plate and tool with triangular pin for different dwell time: (A) dwell time= 2.8 sec, (B) dwell time= 5.6 sec, (C) dwell time= 8.4 sec and (D) dwell time= 11.2 sec.

(A)   (B)
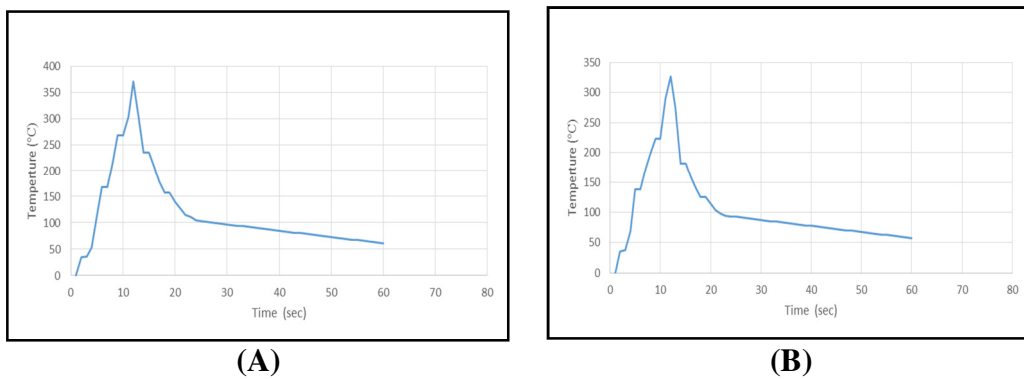
Figure (15) (A): Temperature profile at 4 mm distance from the center of the spot for the cylindrical and (B) Temperature profile at 4 mm distance from the center of the spot for the cylindrical.
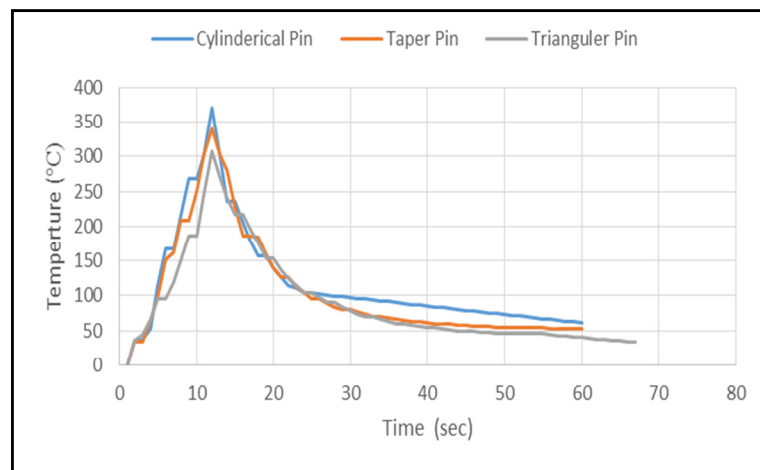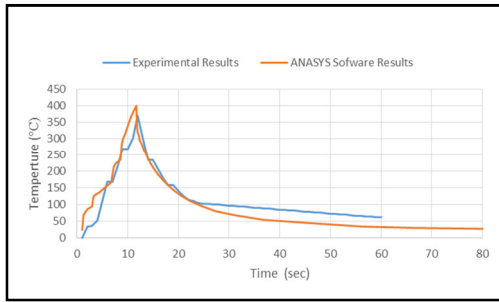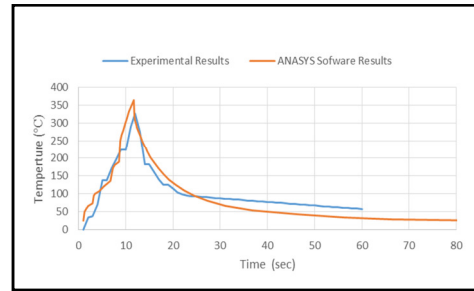

Figure (16) comparison among experimental temperature profiles of the three pin shapes, i.e. cylindrical, tapered and triangular pin.
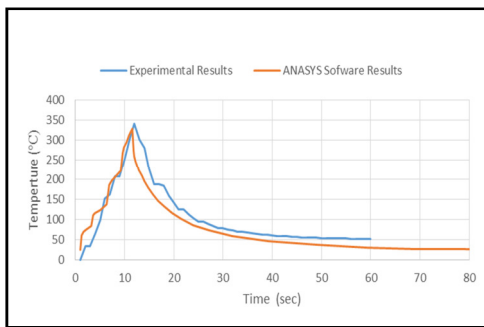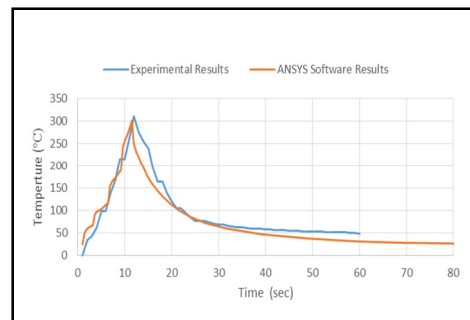
(A)   **(B)**

Figure (17) Comparison between temperature profiles of the experimental and numerical results for cylindrical pin with probe at: (A) a distance 4 mm and (B) at a distance 7 mm from the spot center.
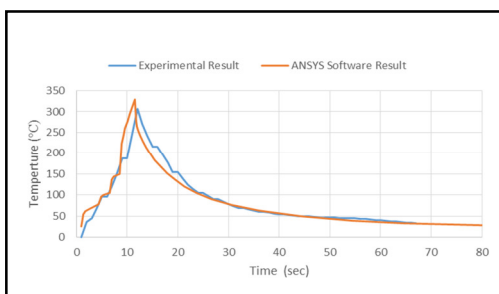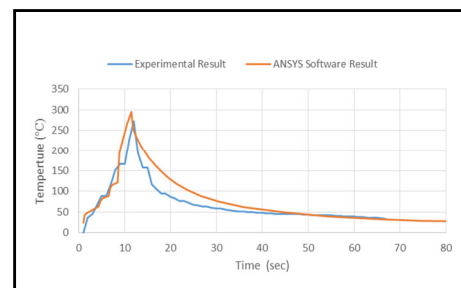

(A)   **(B)**

Figure (18) Comparison between temperature profiles of the experimental and numerical results for tapered pin with probe at: (A) a distance 4 mm and (B) at a distance 7 mm from the spot center.

(A)   **(B)**

Figure (19) Comparison between temperature profiles of the experimental and numerical results for triangular pin with probe at: (A) a distance 4 mm and (B) at a distance 7 mm from the spot center.